ACS APPLIED BIO MATERIALS

www.acsabm.org Article

Green Synthesis and Characterization of Antimicrobial Synergistic AgCl/BAC Nanocolloids

Syed Imdadul Hossain, Maria Chiara Sportelli, Rosaria Anna Picca, Luigi Gentile, Gerardo Palazzo, Nicoletta Ditaranto, and Nicola Cioffi*

Cite This: https://doi.org/10.1021/acsabm.2c00207 Read Online

ACCESS | Metrics & More | Article Recommendations | Supporting Information

ABSTRACT: All over the world, one of the major challenges is the green synthesis of potential materials against antimicrobial resistance and viruses. This study demonstrates a simple method like chemistry lab titration to synthesize green, facile, scalable, reproducible, and stable synergistic silver chloride/benzyldimethylhexadecyl-ammonium chloride (AgCl/BAC) colloidal Nano-antimicrobials (NAMs). Nanocolloidal dispersions of AgCl in an aqueous medium are prepared by using silver nitrate ($AgNO_3$) as precursor and BAC as both sources of chloride and stabilizer, holding an asymmetric molecular structure. The synthetic approach is scalable and green. Both the morphology and stability of AgCl/BAC nanocolloids (NCs) were investigated as a function of different molar fractions of the reagents. AgCl/BAC NCs were characterized by transmission electron microscopy (TEM) and X-ray photoelectron and UV−vis spectroscopies. Zeta potential measurements revealed increasing positive potential values at every stage of the synthesis. Size distribution and hydrodynamic diameter of the particles were measured by dynamic light scattering (DLS), which predicted the formation of BAC layered structures associated with the AgCl nanoparticles (NPs). Small-angle X-ray scattering (SAXS) experiments verify the thickness of the BAC bilayer around AgCl. The produced AgCl/BAC NCs probably have synergistic antimicrobial properties from the AgCl core and the biocide BAC shell. AgCl/BAC NCs stability over months was investigated. The experimental evidence supports the morphological stability of the AgCl/BAC NCs, while higher positive zeta potential values anticipate a long-term antimicrobial effect: a higher surface charge causes NPs to be potentially more lethal to bacteria. AgCl/BAC antimicrobial aqueous colloidal suspensions will be used as additives for the industrial production of antimicrobial coatings.

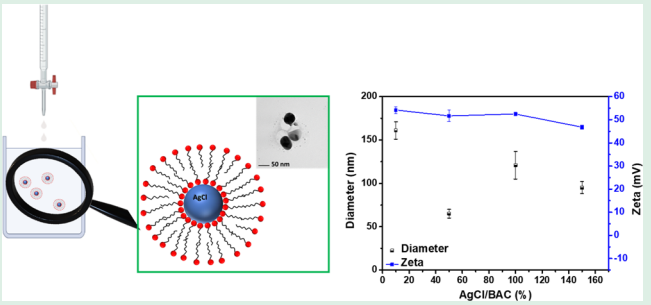

KEYWORDS: *nanoantimicrobials, biofilms, AgCl, colloids, antimicrobial resistance, BAC biocide, SAXS, synergistic*

INTRODUCTION

The current SARS-CoV-2 pandemic and the misuse and overuse of antibiotics by humans are raising fears of new pathogens such as viruses or microbial-resistant bacteria. Alarmingly, more and more infections are becoming resistant to antibiotics. The emerging antimicrobial resistance (AMR) is considered one of the biggest problems to health, food safety, and the economy, leading to higher costs of medical care, prolonged hospital stays, increase mortality rate, and higher unemployment. Recently, the World Health Organization (WHO) outlined that currently available and new-developed antibiotics are not enough to fight against drug-resistant bacteria. On top of that, drug-resistant infections are projected to be responsible for 10 million deaths annually by 2050 worldwide.[1] Unless we take action, we are heading to a post-antibiotic era. This could be an urgent call to put significant effort into innovating technology to prevent, detect, inhibit, and eradicate consortium of bacteria so-called biofilms. In this regard, research communities have drawn attention to develop the next generation biocides and technologies for destroying antibiotic-resistant bacteria and biofilms by engineering the surface texture of nanomaterials.

Various types of NPs such as Ag, Cu, ZnO, CeO_2, TiO_2, Al_2O_3, ZrO_2, Si, SiO_2, Au, CaO, MgO, ceramics, and zeolite are well-known for their antimicrobial property,[2,3] presumably either double or triple heterostructure metal oxide based nanocomposite could be considered as potential against antibacterial resistance. Particularly, Ag-based materials attract special attention as antimicrobial agent because Ag NPs and ions exhibit a wide range of bacteriostatic and biocidal activities against viruses, fungi, and bacteria.[4−10] Ag^+ is found to be active in destroying cellular enzymes and DNA by coordinating to electron-donating groups such as thiols, carboxylates, amides,

Received: March 7, 2022
Accepted: May 31, 2022

imidazoles, indoles, hydroxyls, and so on.[11] Ag shows low cytotoxicity depending on several factors such as size, shape, coating, life cycle, concentration, dosing, particle agglomeration, use of biosafety support, synthetic route, ion release property, and so forth.[12−16] Therefore, Ag-containing materials have been used in real-life applications, for example, in biomedical industries for surgical instrument treatment, dental materials, surface modification of endoprostheses, food industries, wound and burn dressing, additives, personal care products, domestic products (air purifier system), and agricultural products.[17−23] There has been extensive research on synthesis, characterization and applications of AgXs (X = Cl, Br, I). The use of AgXs as photographic materials,[24,25] water splitting, removal of organic wastes and harmful algae are well reported.[26−28] It is also known that nanostructured AgCl, in the presence of an excess of Ag ions, can act as an effective catalyst in the generation of active oxygen species.[29] This feature is highly desirable and could be effective against drug-resistant bacteria and biofilms. Remarkably, AgBr composite was found to be effective in killing both airborne and waterborne bacteria; the AgBr composite surface coating was able to inhibit biofilm growth. Moreover, the study explored a controlled release of biocidal Ag^+ ions from AgBr composites.[30] Several reports outlined the effective use of AgCl NPs in biomedical, cosmetics, and food packaging applications considering antibacterial behavior.[31,32] Silver halides have the potential to be NAMs by providing a tailored concentration of biocidal Ag^+ ions in an aqueous medium. Nonetheless, it is known that AgX salts in pure crystalline form are unstable,[33] whereas AgX salts in a dispersed state are considered stable.[34]

Colloidal stability, convenient synthetic route, nanosafety, antimicrobial activity, and so on, are considered important aspects for the real life application of AgCl NPs. Among many known useful properties, Ag is recognized as an antimicrobial element. Ag NPs is considered extremely shelf stable for long periods of time. Compared to molecular antimicrobials, which are generally targeted to specific organism classes, Ag-based materials are active against diverse range of pathogenic bacteria, fungi, algae, and possibly viruses. Another advantage of Ag antimicrobials is that it can be effortlessly incorporated into many materials such as textiles and plastics, making it especially suitable and sustainable where antimicrobial activity is desirable.[35] The addition of Ag into personal health care product improve hygienic and antimicrobial capacities, and treat skin infection. Moreover, Ag-based dressing improved the efficacy of standard wound dressing, and Ag has been a key component for dental treatment for long time.[36] The majority of Ag-based antimicrobials contain elemental Ag, and this results in very low rate of dissolution in aqueous environment.[37] The use of sparingly soluble AgCl salt in place of elemental Ag could increase the level of control over the generation of biocidal Ag^+, by providing a constant concentration of bioactive Ag^+ ions[30,38] [Ksp (AgCl) 1.76×10^{-10} at 25 °C],[39] while further modulating the release of Ag^+ into the target medium by introducing potential polymer or substrate dispersing matrices.[30] Appropriate solvents, surfactants, and polymers are frequently used to improve the stability and antimicrobial activity of novel metal NPs.[40,41] In this context, polyvinylpyrrolidone (PVP-360) was effective against aggregation of NPs,[41] and various concentrations of polyethylenimine (PEI) showed a significant effect against the agglomeration of colloidal AgNPs.[42] Additionally, poly(vinyl alcohol), poly(methyl vinyl ether), poly(ethylene glycol), dendrimers, and polyamines water-soluble polymers have already been used as stabilizers and protective agents for metal colloids and NPs.[43−47] Notably, AgBr nanocolloids were prepared in aqueous medium, where a quaternary ammonium compound, i.e. hexadecyltrimethylammonium bromide (CTAB) cationic surfactant, acts as both the source of bromide ions and the stabilizing agent. AgBr NPs are thought to be stabilized by a CTAB layered structure.[48] In this regard, previously, Sui et al. studied the effect of CTAB on Ag NPs: the differences between SAXS and TEM results explained the CTAB-NPs interaction; they explored the thickness of CTAB shell layers around NPs.[49] Similarly, sodium dodecyl sulfate (SDS), hexadecyltrimethylammonium chloride (CTAC), and hexadecylpyridinium chloride (CPC) surfactants were used to synthesize a AgCl colloidal suspension in aqueous medium and opened the way to the possible use of BAC to prepare AgCl colloids.[41,50] BAC is an intrinsically safe material which is frequently used as a cosmetic ingredient, biocide, germicide, preservative, hand sanitizer, antiseptic, and disinfectant agent.[51,52] It has been widely used as a stabilizing surfactant of metal NPs aiming at developing a synergistic antibacterial compound.[53] BAC is listed as antibacterial and novel antituberculosis agent by the Johns Hopkins Clinical Compound Library (JHCCL).[54] Apparently, BAC exerts toxic effects on bacteria, and acyl chain length distributions and the degree of C−C saturation of BAC significantly impact on the antimicrobial activity against both Gram-positive and Gram-negative bacteria.[55] Specifically, aromatic moieties of BAC should improve the stability of NPs because of their stacking abilities, which can favor the formation of surfactant bilayers around the NPs.[48] However, to attract attention from the scientific community and to find potential application, further experiments and full characterization should be performed, finding suitable reaction conditions, NPs size distribution, NPs surface charge, chemical state, real-time AgCl formation, colloidal sedimentation, long time stability, reproducibility, low cytotoxicity, ion release property. The novelty of this paper is the green and facile, cost-effective and scalable, reproducible synthesis, and in situ characterization of stable synergistic AgCl/BAC NCs as alternative strategies in the development of nanoantimicrobials (NAMs) to slow down antimicrobial resistance and possible inhibition of biofilms.

Particularly, in this work, a simple chemistry laboratory titration technique was employed to synthesize stable synergistic AgCl/BAC colloidal NAMs. In order to find the best conditions for the production of AgCl/BAC NCs, four different stages of synthesis, such as 10%, 50%, 100%, and 150% titration, were carried out. In the reaction, presumably a silver cation reacts with the chloride counterion of the BAC to form AgCl, while the BA^+ molecules act as a stabilizer. Interestingly, at every stage of synthesis, the system is producing AgCl/BAC NCs. Morphology and size, AgCl/BAC formation and growth, zeta potential measurement, understanding of core−shell structure, chemical state, and stability of the AgCl/BAC NCs were investigated as a function of different molar fractions of the reagents.

MATERIALS AND METHODS

Materials. Silver nitrate ($AgNO_3$) and benzyldimethylhexadecylammonium chloride (BAC) were purchased from Sigma−Aldrich (Milan, Italy). Milli-Q water was used throughout the experiments.

Synthesis of AgCl/BAC NCs. Nanocolloids of AgCl/BAC were prepared by titrating an aqueous solution of $AgNO_3$ into an aqueous BAC solution. Samples were collected at different stages of synthesis for characterization. In brief, a stock solution of 1 mM $AgNO_3$ and 1 mM BAC were prepared in Milli-Q water. Using a P1000 micropipette, a $AgNO_3$ titrating solution was added dropwise (12 drops per minute) to

https://doi.org/10.1021/acsabm.2c00207
ACS Appl. Bio Mater. XXXX, XXX, XXX−XXX

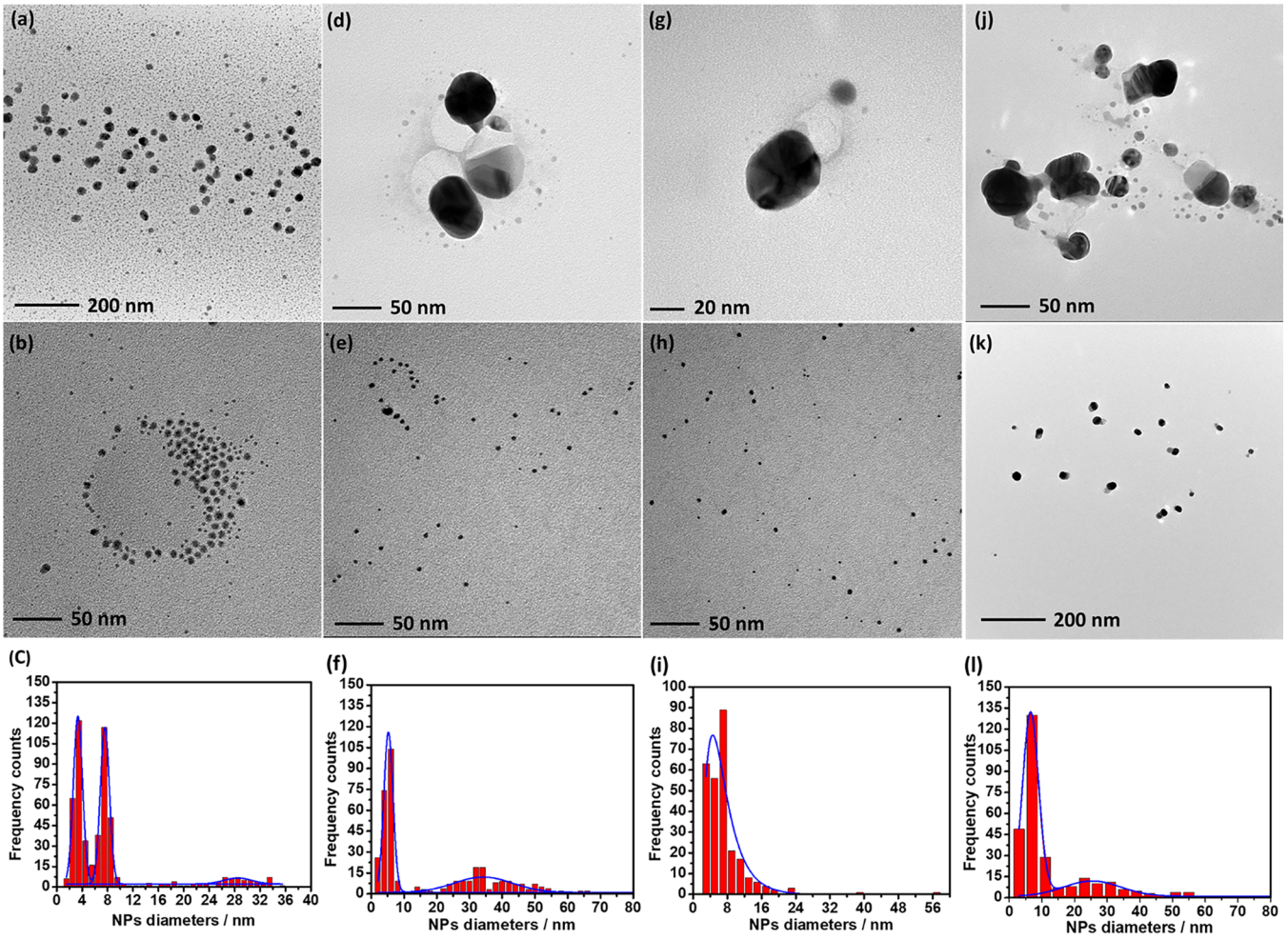

Figure 1. Typical TEM images and histograms of (a–c) AgCl/BAC (10%), (d–f) AgCl/BAC (50%), (g–i) AgCl/BAC (100%), and (j–l) AgCl/BAC (150%) NCs.

the BAC solution under continuous stirring at room temperature. Different fractions of $AgNO_3$ solution were added into BAC solution, i.e., 10%, 50%, 100%, and 150% molar ratios. Light milky color was visible upon addition of Ag ion into BAC surfactant solution, which was a preliminary signal of the formation of AgCl/BAC NCs. The AgCl/BAC containing solution kept under magnetic stirring for 5 min after complete addition of required amount of $AgNO_3$ solution into BAC solution. The AgCl NPs can be isolated as powder form by means of centrifugation at 10 000 rpm.

TEM Morphological Characterization. TEM analysis was performed using a FEI Tecnai 12 instrument (120 kV; filament: LaB_6). NCs were drop-cast on copper grids (Formvar coated, 300 mesh, Agar Scientific) in the volume of 2 to 3 μL, for each AgCl/BAC NCs (10 to 150%). Size distribution analysis was performed with ImageJ software.

DLS and Zeta-Potential Measurements. The Zetasizer Nano ZS instrument (Malvern Instruments, Ltd., Worcestershire, UK) equipped with a 4 mW He–Ne laser and an automatic laser attenuator, and the detector was an avalanche photodiode was used for DLS measurements (at θ = 173°), as well as zeta-potential measurements (at θ = 12.8°). The temperature was set to 25 °C. Two kind of experiments were performed: (i) kinetic experiments and (ii) steady state experiments. (i) Kinetic experiments were performed recording each correlogram for 10 s setting the minimum time in between measurements (resulting in a sampling of ~20 s); (ii) steady-state experiments were performed at the final stage collecting three consecutive DLS (each of them averaged on 11 correlograms). The hydrodynamic radius (R_H) was determined using the Stokes–Einstein eq 1:

$$R_H = \frac{k_B T}{6\pi\eta_s D} \quad (1)$$

where k_B is the Boltzmann constant, T is the temperature, η_s is the solvent viscosity, and D is the diffusion coefficient. The solutions were filled into disposable folded capillary cells (Malvern Instruments), and measurements were performed at a fixed scattering angle of 173° using a laser interferometric technique (laser Doppler electrophoresis) similarly to the kinetic and steady-state experiments described before for the DLS. This technique facilitates determination of the electrophoretic mobility. The electrophoretic mobility can be expressed using Henry's eq 2:[56]

$$u_e = (2\varepsilon_r\varepsilon_0\zeta/3\eta_s)f(\kappa R) \quad (2)$$

where ζ is the zeta potential at the particle surface, ε_r is the dielectric constant of the medium, ε_0 is the permittivity of the vacuum, and η_s denotes the solvent viscosity. The measured electrophoretic mobility values were averaged over three consecutive measurements. The ζ values were calculated using the Hückel approximation.

SAXS Measurements. SAXS experiments were performed using a pinhole-collimated system: SAXSLab Ganesha 300XL instrument (SAXSLAB ApS, Skovlunde, Denmark) equipped with a Genix 3D X-ray source (Xenocs SA, Sassenage, France). The scattering intensity, $I(q)$, was recorded with the Pilatus detector (Dectris Ltd., Baden, Switzerland) located at two distinct distances from the sample, yielding a scattering vector, q, range 0.003 $Å^{-1} \leq q \leq 0.5$ $Å^{-1}$. Samples were loaded in a 1.5 mm diameter quartz capillary and then sealed (Hilgenberg GmbH, Malsfeld, Germany). An external JULABO

https://doi.org/10.1021/acsabm.2c00207
ACS Appl. Bio Mater. XXXX, XXX, XXX–XXX

thermostat (JULABO, Seelbach, Germany) fixed to 25 °C controlled the temperature. The two-dimensional (2D) scattering pattern was radially averaged using SAXSGui v2.15.01 software to obtain $I(q)$. The measured scattering curves were corrected for the background scattering.

Spectroscopic Characterization. Absorption spectra of the AgCl/BAC NCs were carried out using UV−vis spectroscopy (Shimadzu UV-1601), operating the spectrometer between 200 and 600 nm range, in quartz Suprasil cuvettes from Hellma Analytics (Müllheim, Germany). X-ray photoelectron spectroscopy (XPS) analyses were carried out using a PHI 5000 Versa Probe II Scanning XPS Microprobe spectrometer (ULVAC-PHI Inc., Kanagawa, Japan). The measurements were done with a monochromatised Al Kα source (X-ray spot 200 μm), at a power of 50.3 W. Wide scans and detailed spectra were acquired in fixed analyzer transmission (FAT) mode with a pass energy of 117.40 and 46.95 eV, respectively. An electron gun was used for charge compensation (1.0 V 20.0 μA). Calibration of the binding energy (BE) scale was performed by fixing the aliphatic component of the C 1s signal (BE = 284.8 ± 0.1 eV) as reference. Data processing was performed by using the MultiPak software v. 9.9.0.8.

RESULTS AND DISCUSSION

Characterization of AgCl/BAC NCs. The AgCl NCs with synergistic antimicrobial effect were synthesized in aqueous medium by the reaction of $AgNO_3$ and BAC reagents where silver cation reacts with the chloride counterion of the BAC, producing a AgCl core and a BA^+ shell structure. In the system, a $AgNO_3$ aqueous solution was slowly added into BAC solution, observing a transparent solution color changes to light milky color, deducing the production of AgCl NCs. Indeed, adapting an extremely diffused titration approach to the controlled production of aqueous colloidal antimicrobial particles paves the way for the simple, scalable, and green production of antimicrobial colloids, to be used as additives in several technological applications.

The AgCl/BAC morphological characterization was carried out by TEM. Typical micrographs of NPs obtained at four different AgCl/BAC ratios are shown in Figure 1 and confirm the presence of spheroidal AgCl NPs with average diameter of 20 to 30 nm.[57] However, the distribution of particles around such an average varies depending on the reaction conditions. At 10% titration, the starting of the process, the size distribution of the AgCl NPs is found to be polydisperse with two small peaks at 20−30 nm and at 5−10 nm (Figure 1a−c), which probably refers to the formation of a lower number of stable AgCl where BAC micelle are supposed to be dominating. This phenomenon is ascribable to the early stage of the reaction indeed as the reaction progress the multiple distribution is converted into two populations. Upon degree of titration, at 50% titration, higher number of stable polydisperse AgCl NPs with two different average size distribution where one still remaining in higher number in the size range between 20 to 30 nm, as can be seen in Figure 1d−f. At 100% titration with increasing the concentration of $AgNO_3$, a decrease in particle size below 10 nm (Figure 1g−i) was observed in higher number, which could be due to the increase in the number density of the particles and limiting the surfactant molecules in providing sufficient protection to the larger number of NPs. Whereas, 150% titration (Figure 1j−l) is considered a highly unstable stage in producing AgCl/BAC NCs because an excess amount of $AgNO_3$ might overcome the surfactant molecules' shell around the AgCl NPs which causes Ag ions uncovered; consequently, the photodecomposition occurs under visible light.

Nonetheless, further investigation is needed in order to confirm our hypothesis on the formation of BAC around AgCl NPs by evaluating the hydrodynamic radius of AgCl/BAC NPs including AgCl inorganic core and BA organic shell (surfactant molecules) as can be seen in Figure 2. Dynamic light scattering

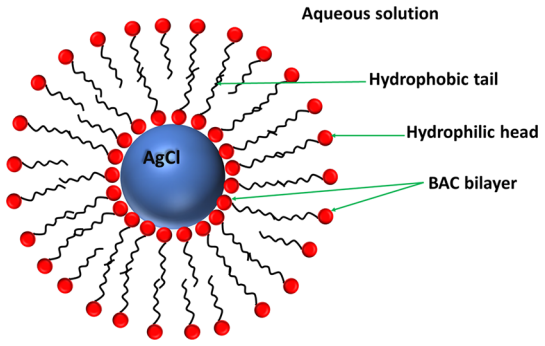

Figure 2. Schematic model for AgCl NPs stabilized by BA^+ molecules.

(DLS) measurements suggest the formation of BAC layered structures as shell around the AgCl NPs core, since the number-weighted hydrodynamic diameter, $d_H = 2R_H$ (Figure 3a), is more than 3 times higher than the TEM diameter (Figure 1). Divergence between DLS and TEM size determination of inorganic nanoparticles is well-known, DLS mean diameter should be 20−30% higher than TEM mean size.[58,59]

Figure 3a shows DLS size distribution of NCs for different AgCl/BAC ratios. The sharp peak of size distribution indicates that the system started showing a narrow size distribution and particles were same size and uniform at 50% titration, which also supports the statement of the formation of higher number of stable AgCl NPs (well agreement with TEM histogram as shown in Figure 1f) than at 10% titration where micelles are dominating over a limited number of AgCl NPs. The system should reach stoichiometric completion at 100% titration, which presumably indicates the absence of excessive Ag ions and chloride. In the experiment, 1 mM BAC is used, which is lower than the BAC critical micellar concentration (CMC) (5 and/or 5.2 mM).[60−62] DLS and zeta potential measurements of bare BAC solution at the same concentration (1 mM) can be seen in Figure S1. The derived count rate, i.e. absolute intensity, for the BAC sample is 500 ± 30 kcps, while the derived count rate for the AgCl/BAC (50%) goes from 28 000 to 350 000 kcps (Figure 7), aggregates in the BAC at 1 mM are negligible with respect to our purpose. According to the maximum number % of size and zeta potential plot (Figure 3b), the system had an optimum condition at 50% titration. The number-average diameter values of AgCl/BAC (10%), AgCl/BAC (50%), AgCl/BAC (100%), and AgCl/BAC (150%) NCs were 161 ± 10, 65 ± 5, 121 ± 16, and 95 ± 7 nm, respectively (Table 2). Besides, zeta potential measurements were performed to find the overall surface potential of NPs because of the result of different amounts of counterions, which could bring the information on bioactivity of AgCl/BAC NCs. Noticeably, higher positive zeta potential values more than 50 mV were found at every stage of the synthesis, which provide information on the long time stability of NCs considering the rule of thumb that zeta potential values higher than 30 mV are sufficient to prevent colloid aggregation.[63] However, the system predicts a long-term antimicrobial effect as higher surface charge causes NPs to be more lethal to bacteria.[64,65] This statement is valid except for 150% titration, where an excess of $AgNO_3$ might cause a reduction of zeta potential value.

In the following, SAXS measurements are proposed to elucidate this discussion (Figure 4). The 1D-averaged SAXS

https://doi.org/10.1021/acsabm.2c00207
ACS Appl. Bio Mater. XXXX, XXX, XXX−XXX

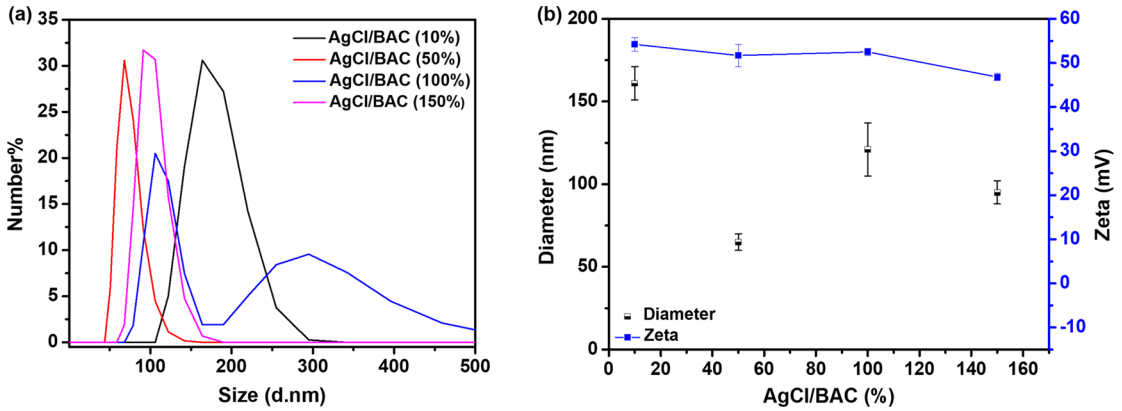

Figure 3. (a) Size distribution by number % and (b) maximum number % of size and zeta potential values of AgCl/BAC (10−150%).

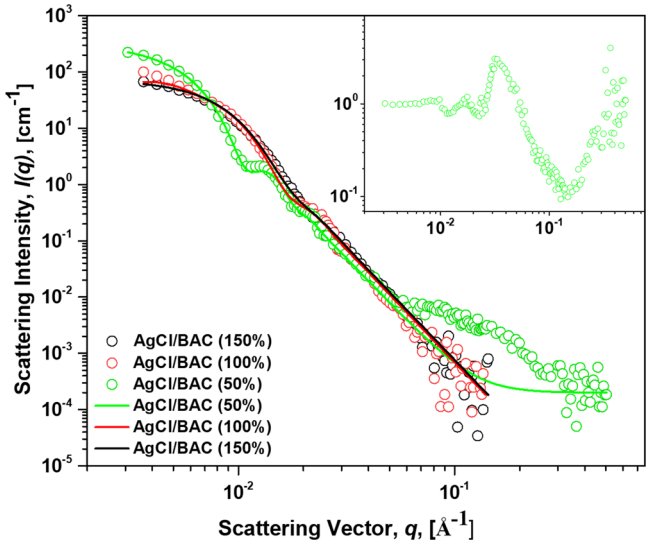

Figure 4. 1D averaged small-angle X-ray scattering profiles of AgCl/BAC (50%), AgCl/BAC (100%), and AgCl/BAC (150%). The solid lines are the core−shell sphere model fitting profiles, while the inset is the $I(q)$ profile of AgCl/BAC (50%) divided for the corresponding model profile.

profiles of 50, 100, and 150% titration in Figure 4 can be interpreted in terms of polydisperse core−shell spheres, where the form factor $\langle P(q)_{CS}\rangle$ is[66]

$$\langle P(q)_{CS}\rangle = \frac{\varphi}{V_S}\left[3V_C(\rho_C - \rho_S)\frac{[\sin(q\langle R_C\rangle)] - qR_C\cos(q\langle R_C\rangle)}{(q\langle R_C\rangle)^3} + 3V_S(\rho_S - \rho_{solv})\frac{[\sin(q(\langle R_C\rangle + \langle\delta\rangle))] - q(\langle R_C\rangle + \langle\delta\rangle)\cos(q(\langle R_C\rangle + \langle\delta\rangle))}{(q(\langle R_C\rangle + \langle\delta\rangle))^3}\right]^2 + b \quad (3)$$

Here, $<P(q)_{CS}>$ describes the nanoparticles, modeled as polydisperse spheres having an average core radius $<R_C>$ and an average thickness $\langle\delta\rangle$, a polydispersity is applied to both with a Shultz distribution.[67] ϕ is the volume fraction of the particles, V_S and V_C are the volume of the whole particle considering as radius the sum of the core radius and the shell thickness (R_C+δ) and the core radius, R_C, respectively. ρ_C, ρ_{CS}, and ρ_{solv} are the scattering length densities of the core, shell, and solvent, respectively. b is the background. Table 1 reports all parameters. The radius of gyration of a core−shell particle can be obtained by using eq 4.

$$R_g^2 = \frac{3}{5}(R_C + \delta)^2\left\{\frac{\left[\frac{(\rho_C - \rho_S)}{(\rho_S - \rho_{solv})}\left(\frac{R_C^5}{(R_C+\delta)^5}\right)\right] - 1}{\left[\frac{(\rho_C - \rho_S)}{(\rho_S - \rho_{solv})}\left(\frac{R_C^3}{(R_C+\delta)^3}\right)\right] - 1}\right\} \quad (4)$$

There are several important observations from the SAXS data: (i) The core radius decreases with increasing particle density in agreement with TEM (Figure 1) and literature;[68] (ii) From AgCl/BAC (50%) to AgCl/BAC (100%), the shell thickness adopted is very close to a BAC bilayer; (iii) Polydispersity increases by increasing the $AgNO_3$/BAC ratio; (iv) At AgCl/BAC (50%) and AgCl/BAC (100%) samples, there is a

Table 1. Parameters Utilized in eq 3 to Simulate Scattering Profiles of Figure 4[a]

samples	AgCl/BAC (50%)	AgCl/BAC (100%)	AgCl/BAC (150%)
volume fraction, ϕ	3×10^{-6}	3.8×10^{-6}	3.4×10^{-6}
core radius, R_C	390 Å	250 Å	220 Å
polydispersity of R_C	15%	22%	25%
shell thickness, δ	42 Å	42 Å	42 Å
polydispersity of δ	15%	22%	25%
SLD core, ρ_C	42×10^{-6} Å^{-2}	42×10^{-6} Å^{-2}	42×10^{-6} Å^{-2}
SLD shell, ρ_S	9.25×10^{-6} Å^{-2}	9.25×10^{-6} Å^{-2}	9.25×10^{-6} Å^{-2}
SLD solvent, ρ_{solv}	9.46×10^{-6} Å^{-2}	9.46×10^{-6} Å^{-2}	9.46×10^{-6} Å^{-2}
radius of gyration, R_g	302 Å	226 Å	203 Å

[a]The radius of gyration is obtained by using eq 4.

https://doi.org/10.1021/acsabm.2c00207
ACS Appl. Bio Mater. XXXX, XXX, XXX−XXX

Table 2. Analysis of Ag 3d and Cl 2p Photoelectron Peaks, Ag MNN Auger Peaks, and Z-Average for AgCl/BAC (10%), AgCl/BAC (50%), AgCl/BAC (100%), and AgCl/BAC (150%) NCs[a]

	Ag $3d_{5/2}$ (eV)		Cl $2p_{3/2}$ (eV)			
samples	including error	with reference values	including error	with reference values	α' (eV)	Z-average (nm)
AgCl/BAC (10%)	367.8 ± 0.2	367.8 ± 0.1	198.9 ± 0.2	198.9 ± 0.5	724.4 ± 0.3	161 ± 10
AgCl/BAC (50%)	367.6 ± 0.2	367.6 ± 0.1	199.4 ± 0.2	199.4 ± 0.2	723.8 ± 0.3	65 ± 5
AgCl/BAC (100%)	367.8 ± 0.2	367.8 ± 0.1	199.5 ± 0.3	199.5 ± 0.2	724.2 ± 0.3	121 ± 16
AgCl/BAC (150%)	367.6 ± 0.2	367.6 ± 0.1	199.3 ± 0.3	199.3 ± 0.2	724.0 ± 0.3	95 ± 7

[a]Standard error was calculated on the basis of three different spot values.

secondary structure superposed to the form factor of the nanoparticles ascribed to BAC micelles. Finally, Rg is close to the TEM size estimation in the error bar.

It is thought by scientists that quaternary ammonium chlorides' (QACs) surfactant molecules may stabilize metal clusters through binding of headgroups on the particles surface. In this regard, Sui et al. showed that the binding between QAC and Ag surface occurs via headgroups in aqueous medium.[69] This situation could be real as to the presence of excess of chloride ion, namely, in 10%, 50%, and 100% titration stage. Herein, the positive zeta-potential and the SAXS evidence presumably refers that the head of one BAC interacts with the surface of the Ag, while the tail is interacting with the tail of a second BAC molecule (Figure 2) resulting in a final positively charged surface because of the head of the second surfactant. In the case of 50%, the excess free surfactant leads to surfactant micelles that can be observed in the SAXS profile surface because of the head of the second surfactant.

UV−vis absorption spectra of AgCl/BAC are found to be well in agreement with DLS data and confirm the presence of AgCl for all fraction of AgCl/BAC NCs which can be seen in Figure 5a. Colloidal dispersion exhibited strong and intense peak at around 260 nm and absorbance increases apparently with increasing percentage of titration. At 10% titration, the wavelengths at 256 ± 2 nm, 262 ± 2 nm, and 268 ± 2 nm might be arising from BAC aqueous solution. The absorption spectrum of AgCl/BAC (10%) is almost identical to the bare BAC solution. In this system, likely few and small AgCl NPs are surrounded by BAC molecules. A strong and intense peak at 256 ± 2 and 268 ± 2 nm was observed, respectively, at 50% and 100% titration, which could be attributed to the presence of BA^+-coated AgCl NPs.[50,70,71] The large bands appearing around 260 nm from 50% to 150% samples, probably due to the formation of higher number of stable AgCl (a hypothesis which is in agreement with TEM and DLS), which is intrinsic absorption of AgCl.[72] At 150% titration, the peak at around 270 nm appeared faint, which could be due to a lower amount of BAC molecules in providing sufficient protection to the larger number of AgCl NPs and the presence of an excess of free Ag^+ ions. In principle, AgCl NPs have high direct and indirect band gap, resulting in no absorbance in the visible region but exhibiting a strong signal in the ultraviolet region (200−300 nm).[72−75] Further, the optical band gap is calculated by plotting the relation between $(\varepsilon h\nu)^2$ and hv (Figure S2). From the intercept and slope of the linear part of the plot the direct band gap for AgCl/BAC (10%), AgCl/BAC (50%), AgCl/BAC (100%), AgCl/BAC (150%) was estimated to be around 5.6 eV, which is in agreement with the values of the AgCl NPs band gap reported in the literature (5.6 eV).[75,76] It is worth noting that, at every stage of reaction, colloidal dispersions containing AgCl do not exhibit a surface plasmon resonance peak (SPR) around 400 nm, which implies that BAC stabilizing agent protects the AgCl colloids from photo reduction to Ag^0. Furthermore, light milky color (Figure 5b inset) is found to be visible upon addition of $AgNO_3$ into BAC surfactant solution, which is also in agreement with the formation of AgCl/BAC NCs.

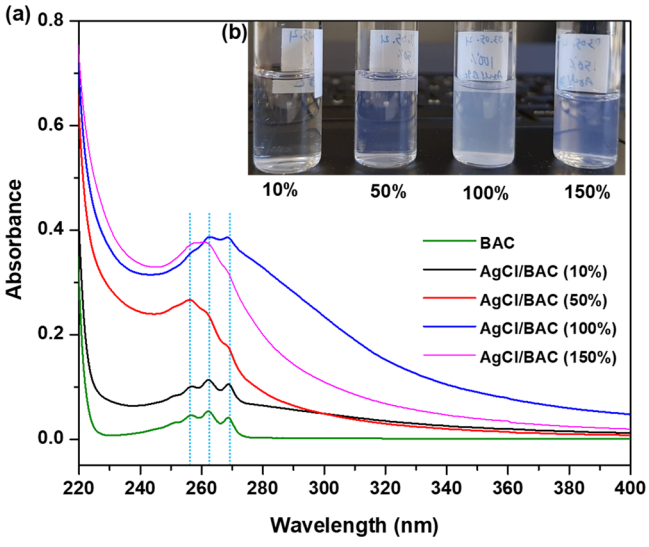

Figure 5. (a) UV−vis absorption spectra of BAC, AgCl/BAC (10%), AgCl/BAC (50%), AgCl/BAC (100%), and AgCl/BAC (150%). (b) Color changes of AgCl/BAC NCs at different titration stages (10−150%).

Further information on the chemical state of AgCl/BAC is provided by XPS analysis. AgCl/BAC surface chemical speciation was achieved by fitting both Ag main photoelectronic and Auger signals (Figure 6a,b). The analyzed results are summarized in Table 2. The modified Auger parameter (α'),[77] calculated as the sum of binding energy BE(Ag $3d_{5/2}$) and the kinetic energy KE(Auger) of the $M_4N_{45}N_{45}$ sharpest peak, was used to assess the AgCl/BAC surface chemical speciation. The α' value of AgCl/BAC (50%) is found to be in agreement with the presence of AgCl (723.8 ± 0.5 eV)[78] and Ag_2O (723.8 ± 0.3 eV),[79] while Ag $3d_{5/2}$ centered at 367.6 ± 0.1 eV (Figure 6a) also represents AgCl phase.[80,81] C 1s spectrum of AgCl/BAC (50%), reported as Figure S3 in the Supporting Information, shows three different chemical components. The first peak can be attributed to the C−C, C═C, and C−H aromatic bonds with characteristic binding energy of (284.8 ± 0.2 eV).[82] The second peak may be assigned to the carbon atoms bonded to nitrogen in C−N bonds at (285.9 ± 0.3) eV, or C−OH from environmental contamination. The third peak may be ascribed to the carbon atom of the C═O bond, arising from adventitious contamination. In terms of AgCl/BAC (10%), AgCl/BAC (100%), and AgCl/BAC (150%) NCs, Ag $3d_{5/2}$ showed peaks at 367.8 ± 0.1 eV, 367.8 ± 0.1 eV, and 367.6 ± 0.1 eV, respectively, which

https://doi.org/10.1021/acsabm.2c00207
ACS Appl. Bio Mater. XXXX, XXX, XXX−XXX

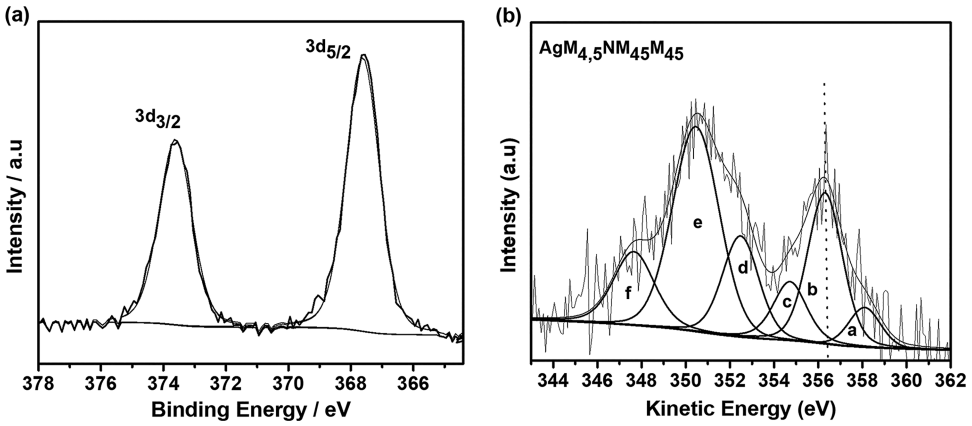

Figure 6. (a) Ag 3d XPS and (b) AgMNN Auger spectra of AgCl/BAC (50%).

indicate the presence of AgCl in the NCs. Moreover, the α' of AgCl/BAC (10%) (724.4 ± 0.5 eV), AgCl/BAC (100%) (724.2 ± 0.5 eV), and AgCl/BAC (150%) (724.0 ± 0.5 eV) corroborate the hypothesis of the formation of AgCl in the system at every stage of reaction.[80,81] However, the acquired Ag 3d core photoelectron peaks and α' values of the AgCl/BAC NCs also indicate the presence of Ag_2O, which is ascribable to the storage condition due to oxygen absorption by AgCl samples at the solid state. This result is not unexpected upon air exposure and does not affect the real-life application of the as-prepared AgCl/BAC NPs, which will release biocidal Ag^+ ions into the surrounding medium as well, aiming at a long-lasting antimicrobial effect.

Kinetics Growth, Stability, and Antimicrobial Property of AgCl/BAC NCs over Time. According to TEM and DLS characterization of AgCl/BAC NCs, AgCl/BAC (50%) was found to be best ratio in terms of stability and particle size, with an average diameter of 30 nm as observed by TEM. A hydrodynamic radius of 65 nm (number-average), including the core AgCl and the BA^+ shell, and a higher positive zeta potential value were found. Moreover, presence of optimum number of Ag^+ ions in AgCl/BAC (50%) might be effective in producing reactive oxygen species while extra sufficient aromatic moieties of BAC can improve stability of AgCl NPs. The balance between Ag^+ ions and BAC moieties is achieved in AgCl/BAC(50%) stage of reaction. Therefore, the kinetics of the AgCl/BAC NPs growth in AgCl/BAC (50%) system was studied by DLS as a function of time. AgCl/BAC (Z- average 65 ± 5 nm) started forming within 50 s of reaction and remained stable in particle size between 50 and 70 nm Z-average as can be seen in Figure 7. In the meantime, the stability of the colloids is evaluated by checking the stability of the derived count rate vs time from repeated DLS measurement of colloids. Aggregation of NPs in colloidal solution could be monitored by observing the sedimentation of colloids. Observation of NPs sedimentation in colloids is also useful to understand the size distribution and stability of NPs in colloidal solution.[83,84] Sedimentation of colloids is a natural phenomenon occurring in colloidal solutions; the NPs sedimentation rate is dependent on particle/aggregate size and density. In aqueous solutions, surfactant addition should lower the sedimentation rates because of its stabilizing effect with respect to aggregation.[85] In this view, at the AgCl/BAC (50%) colloidal system, an increasing derived count rate with less fluctuation (Figure 7) explained the much slower sedimentation rate.

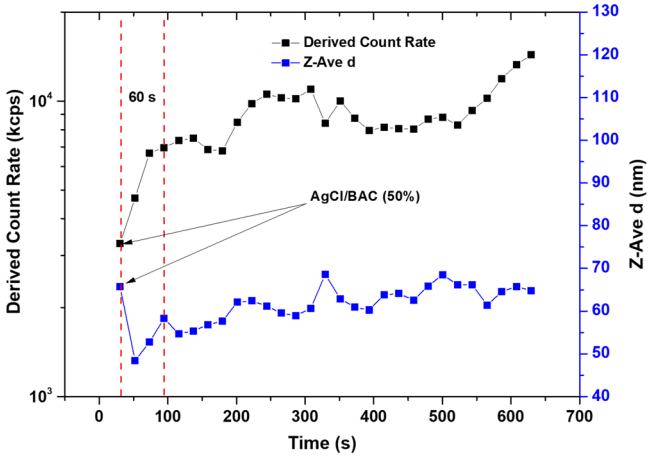

Figure 7. Kinetics of the growth of AgCl/BAC (50%) NCs derived count rate Vs Time.

NPs and bacteria interaction is driven mostly by van der Waals, dipole, and electrostatic interactions. The bacteria−NPs electrostatic interactions are strongly dependent on surface potential differences. Most of the bacteria exhibit a negative zeta potential.[86] Hence, it is vital to measure the surface potential of AgCl/BAC NPs. To evaluate the long-term stability, a 30-days-aged AgCl/BAC(50%) NCs sample was compared with a freshly prepared one. A minor change in size distribution curve was noticed, as shown in Figure S4a. Hence, the AgCl NPs retain R_H for a long time. The zeta potential value is found at 51.5 ± 2.5 mV and 46.5 ± 2.0 mV for fresh and aged samples, respectively, as shown in Figure S4b. In colloidal systems, electrostatic interactions among NPs is considered an important parameter to determine colloidal stability.[63] With this view, 60-days-aged AgCl/BAC (50%) NC was subjected to TEM characterization. The TEM images (Figure S5) of AgCl NPs provide information on dipole and electrostatic interactions among NPs.[87] NPs organize in "lines" with negligible aggregation; this phenomenon further confirms the presence of dipole interactions between BA^+-capped particles. Furthermore, UV−vis spectra (Figure S6a) of fresh AgCl/BAC (50%) colloidal dispersion were recorded and exhibited a strong and intense peak at 256 ± 2 nm, and upon 90 days of storage, a minor shift of ∼8 nm was observed. This means that BAC molecules still protect AgCl from photodecomposition. Additionally, photographs (Figure S6b, inset) compare fresh and aged samples, and aged samples retain a light milky color even after 90 days of aging. The

https://doi.org/10.1021/acsabm.2c00207
ACS Appl. Bio Mater. XXXX, XXX, XXX−XXX

advantage of limited solubility of AgCl enables the AgCl/BAC system to be active for a long time. For instance, almost a year aged AgCl/BAC (100%) NC was stored at room temperature then the sample exposed to TEM characterization. Interestingly, insignificant aggregation and electrostatic interaction among AgCl NPs is observed as presented in Figure S7.

CONCLUSIONS

In this paper, we have proposed a green and facile route in producing highly stable, reproducible, and scalable NAMs with highly positive zeta potential values. TEM, XPS, and UV−vis characterizations confirm the presence of AgCl NPs. Furthermore, TEM, DLS and UV−vis characterizations confirm a good colloidal stability up to 90 days of storage, thanks to the presence of BAC molecules which provide protection to AgCl NPs from aggregation and decomposition. DLS was used to observe in real time AgCl NPs formation surrounded by BA^+ species, along with excess Ag^+ ions. DLS size distribution and hydrodynamic diameter, along with kinetics of the particle growth, predicted the formation of BAC layered structures around NPs. The latter was supported by SAXS measurements, which suggest the formation of AgCl-BAC NPs as core−shell structures in the aqueous medium. Further investigation on long-time aged samples and frequently repeated experiments demonstrated the stability and reproducibility of the AgCl/BAC NCs. Application of the as-prepared AgCl/BAC NCs for the development of antimicrobial water-insoluble hard coatings, in either bioactive polymers or clay as substrates, providing slow-releasing active phases, is planned. These material could have potential use either in the production of active food packaging or biosafe biomedical devices, with long-lasting antimicrobial properties.

ASSOCIATED CONTENT

Supporting Information

The Supporting Information is available free of charge at https://pubs.acs.org/doi/10.1021/acsabm.2c00207.

(i) Tauc plots and other details on the nanoparticle direct band gap calculation; (ii) DLS size distribution by number % and zeta potential measurements of BAC solutions (1 mM); (iii) C 1s XPS spectra of AgCl/BAC (50%); (iv) Size distribution by number% and zeta potential values of aged AgCl/BAC (50%) NCs; (v) TEM images of fresh and aged AgCl/BAC (50%) NCs; (vi) UV−vis absorption spectra and photographs of fresh and aged AgCl/BAC (50%) NCs; (vii) TEM images of 1 year aged AgCl/BAC (100%) NCs (PDF)

AUTHOR INFORMATION

Corresponding Author

Nicola Cioffi − *Chemistry Department, University of Bari "Aldo Moro", 70126 Bari, Italy; CSGI (Center for Colloid and Surface Science) c/o Dept. Chemistry, 70125 Bari, Italy;* orcid.org/0000-0002-6765-440X; Email: nicola.cioffi@uniba.it; Fax: +39 080 544 2026

Authors

Syed Imdadul Hossain − *Chemistry Department, University of Bari "Aldo Moro", 70126 Bari, Italy; CSGI (Center for Colloid and Surface Science) c/o Dept. Chemistry, 70125 Bari, Italy;* orcid.org/0000-0001-5502-3806

Maria Chiara Sportelli − *Chemistry Department, University of Bari "Aldo Moro", 70126 Bari, Italy;* orcid.org/0000-0002-8832-2770

Rosaria Anna Picca − *Chemistry Department, University of Bari "Aldo Moro", 70126 Bari, Italy; CSGI (Center for Colloid and Surface Science) c/o Dept. Chemistry, 70125 Bari, Italy;* orcid.org/0000-0001-8033-098X

Luigi Gentile − *Chemistry Department, University of Bari "Aldo Moro", 70126 Bari, Italy; CSGI (Center for Colloid and Surface Science) c/o Dept. Chemistry, 70125 Bari, Italy;* orcid.org/0000-0001-6854-2963

Gerardo Palazzo − *Chemistry Department, University of Bari "Aldo Moro", 70126 Bari, Italy; CSGI (Center for Colloid and Surface Science) c/o Dept. Chemistry, 70125 Bari, Italy;* orcid.org/0000-0001-5504-2177

Nicoletta Ditaranto − *Chemistry Department, University of Bari "Aldo Moro", 70126 Bari, Italy; CSGI (Center for Colloid and Surface Science) c/o Dept. Chemistry, 70125 Bari, Italy*

Complete contact information is available at: https://pubs.acs.org/10.1021/acsabm.2c00207

Author Contributions

S.I.H. performed all the syntheses and most of the characterization experiments, and wrote the first draft of the manuscript. M.C.S. performed TEM analyses and corresponding data treatment, and took part in manuscript revision. R.A.P. took part in data treatment and interpretation, and in manuscript revision. L.G. performed SAXS experiments and corresponding data treatment, and took part in manuscript revision. G.P. took part in scientific discussion regarding DLS and z-potential measurements, and took part in manuscript revision. N.D. performed XPS analyses and corresponding data treatment, and took part in manuscript revision. N.C. took part in scientific discussions, refined the different sections of this paper, and coordinated the study.The manuscript was written through contributions of all authors. All authors have given approval to the final version of the manuscript.

Notes

The authors declare no competing financial interest.

ACKNOWLEDGMENTS

Financial support is acknowledged from European Union's 2020 research and innovation program under the Marie Sklodowska-Curie Grant Agreement No. 813439. M.C.S. acknowledges the financial support from Fondo Sociale Europeo "Research for Innovation (REFIN)"; project n° 435A866B.

REFERENCES

(1) Jack, A.; Campbell, C. The threat of antibiotic resistance — in charts https://www.ft.com/content/d806dcf5-23f8-4714-ad04-ca11a66061e2 (accessed January 23, 2021).

(2) Dizaj, S. M.; Lotfipour, F.; Barzegar-Jalali, M.; Zarrintan, M. H.; Adibkia, K. Antimicrobial Activity of the Metals and Metal Oxide Nanoparticles. *Materials Science and Engineering: C* **2014**, *44*, 278−284.

(3) Rhim, J.-W.; Hong, S.-I.; Park, H.-M.; Ng, P. K. W. Preparation and Characterization of Chitosan-Based Nanocomposite Films with Antimicrobial Activity. *J. Agric. Food Chem.* **2006**, *54* (16), 5814−5822.

(4) Zachariadis, P. C.; Hadjikakou, S. K.; Hadjiliadis, N.; Skoulika, S.; Michaelides, A.; Balzarini, J.; De Clercq, E. Synthesis, Characterization and in Vitro Study of the Cytostatic and Antiviral Activity of New Polymeric Silver(I) Complexes with Ribbon Structures Derived from

the Conjugated Heterocyclic Thioamide 2-Mercapto-3,4,5,6-tetrahydropyrimidine. *Eur. J. Inorg. Chem.* **2004**, *2004*, 1420−1426.
(5) Bragg, P. D.; Rainnie, D. J. The Effect of Silver Ions on the Respiratory Chain of Escherichia Coli. *Can. J. Microbiol.* **1974**, *20*, 883.
(6) Pallavicini, P.; Dacarro, G.; Taglietti, A. Self-Assembled Monolayers of Silver Nanoparticles: From Intrinsic to Switchable Inorganic Antibacterial Surfaces. *Eur. J. Inorg. Chem.* **2018**, *2018* (45), 4846−4855.
(7) Chernousova, S.; Epple, P. D. M. Silver as Antibacterial Agent: Ion, Nanoparticle, and Metal. *Angewandte Chemie International Edition* **2012**, *52* (6), 1636−1653.
(8) Zheng, K.; Setyawati, M. I.; Leong, D. T.; Xie, J. Antimicrobial silver nanomaterials. *Coordination Chemistry Reviews* **2018**, *357*, 1−17.
(9) Kukushkina, E. A.; Hossain, S. I.; Sportelli, M. C.; Ditaranto, N.; Picca, R. A.; Cioffi, N. Ag based synergistic antimicrobial composites. A critical review. *Nanomaterials* **2021**, *11* (7), 1687.
(10) Tehri, N.; Vashishth, A.; Gahlaut, A.; Hooda, V. Biosynthesis, antimicrobial spectra and applications of silver nanoparticles: current progress and future prospects. *Inorganic and Nano-Metal Chemistry* **2020**, *52* (1), 1−19.
(11) Holt, K. B.; Bard, A. J. Interaction of Silver(I) Ions with the Respiratory Chain of Escherichia coli: An Electrochemical and Scanning Electrochemical Microscopy Study of the Antimicrobial Mechanism of Micromolar Ag^{+}. *Biochemistry* **2005**, *44* (39), 13214−13223.
(12) Ferdous, Z.; Nemmar, A. Health Impact of Silver Nanoparticles: A Review of the Biodistribution and Toxicity Following Various Routes of Exposure. *International Journal of Molecular Sciences* **2020**, *21* (7), 2375.
(13) Suresh, A. K.; Pelletier, D. A.; Wang, W.; Morrell-Falvey, J. L.; Gu, B.; Doktycz, M. J. Cytotoxicity Induced by Engineered Silver Nanocrystallites Is Dependent on Surface Coatings and Cell Types. *Langmuir* **2012**, *28* (5), 2727−2735.
(14) Lokina, S.; Stephen, A.; Kaviyarasan, V.; Arulvasu, C.; Narayanan, V. Cytotoxicity and Antimicrobial Activities of Green Synthesized Silver Nanoparticles. *Eur. J. Med. Chem.* **2014**, *76*, 256−263.
(15) Lv, H.; Cui, S.; Yang, Q.; Song, X.; Wang, D.; Hu, J.; Zhou, Y.; Liu, Y. AgNPs-Incorporated Nanofiber Mats: Relationship between AgNPs Size/Content, Silver Release, Cytotoxicity, and Antibacterial Activity. *Materials Science and Engineering: C* **2021**, *118*, 111331.
(16) Sportelli, M. C.; Tütüncü, E.; Picca, R. A.; Valentini, M.; Valentini, A.; Kranz, C.; Mizaikoff, B.; Barth, H.; Cioffi, N. Inhibiting P. fluorescens biofilms with fluoropolymer-embedded silver nanoparticles: an in-situ spectroscopic study. *Scientific Report* **2017**, *7*, 11870.
(17) Turner, R. D.; Wingham, J. R.; Paterson, T. E.; Shepherd, J.; Majewski, C. Use of Silver-Based Additives for the Development of Antibacterial Functionality in Laser Sintered Polyamide 12 Parts. *Sci. Rep* **2020**, *10* (1), 892.
(18) de Campos, M. R.; Botelho, A. L.; dos Reis, A. C. Nanostructured Silver Vanadate Decorated with Silver Particles and Their Applicability in Dental Materials: A Scope Review. *Heliyon* **2021**, *7* (6), No. e07168.
(19) Hardes, J.; Ahrens, H.; Gebert, C.; Streitbuerger, A.; Buerger, H.; Erren, M.; Gunsel, A.; Wedemeyer, C.; Saxler, G.; Winkelmann, W.; Gosheger, G. Lack of Toxicological Side-Effects in Silver-Coated Megaprostheses in Humans. *Biomaterials* **2007**, *28* (18), 2869−2875.
(20) Kumar, S.; Basumatary, I. B.; Sudhani, H. P. K.; Bajpai, V. K.; Chen, L.; Shukla, S.; Mukherjee, A. Plant Extract Mediated Silver Nanoparticles and Their Applications as Antimicrobials and in Sustainable Food Packaging: A State-of-the-Art Review. *Trends in Food Science & Technology* **2021**, *112*, 651−666.
(21) Sportelli, M. C.; Ancona, A.; Volpe, A.; Gaudiuso, C.; Lavicita, V.; Miceli, V.; Conte, A.; Del Nobile, M. A.; Cioffi, N. A New Nanocomposite Packaging Based on LASiS-Generated AgNPs for the Preservation of Apple Juice. *Antibiotics* **2021**, *10* (7), 760.
(22) Shao, J.; Cui, Y.; Liang, Y.; Liu, H.; Ma, B.; Ge, S. Unilateral Silver-Loaded Silk Fibroin Difunctional Membranes as Antibacterial Wound Dressings. *ACS Omega* **2021**, *6* (27), 17555−17565.
(23) Sim, W.; Barnard, R. T.; Blaskovich, M. A. T.; Ziora, Z. M. Antimicrobial Silver in Medicinal and Consumer Applications: A Patent Review of the Past Decade (2007−2017). *Antibiotics (Basel)* **2018**, *7* (4), 93.
(24) Hamilton, J. F. The silver halide photographic process. *Adv. Phys.* **1988**, *37* (4), 359−441.
(25) Kuramochi, M.; Omata, H.; Ishihara, M.; Hanslin, S. Ø.; Mizumaki, M.; Kawamura, N.; Osawa, H.; Suzuki, M.; Mio, K.; Sekiguchi, H.; Sasaki, Y. C. Tilting and Rotational Motions of Silver Halide Crystal with Diffracted X-Ray Blinking. *Sci. Rep* **2021**, *11* (1), 4097.
(26) Currao, A.; Raja Reddy, V.; van Veen, M. K.; Schropp, R. E. I.; Calzaferri, G. Water Splitting with Silver Chloride Photoanodes and Amorphous Silicon Solar Cells. *Photochem. Photobiol. Sci.* **2004**, *3* (11−12), 1017−1025.
(27) Reddy, V. R.; Currao, A.; Calzaferri, G. Zeolite A and Zeolite L Monolayers Modified with AgCl as Photocatalyst for Water Oxidation to O2. *J. Mater. Chem.* **2007**, *17* (34), 3603−3609.
(28) Fan, G.; Chen, Z.; Yan, Z.; Du, B.; Pang, H.; Tang, D.; Luo, J.; Lin, J. Efficient Integration of Plasmonic Ag/AgCl with Perovskite-Type LaFeO3: Enhanced Visible-Light Photocatalytic Activity for Removal of Harmful Algae. *Journal of Hazardous Materials* **2021**, *409*, 125018.
(29) Schürch, D.; Currao, A.; Sarkar, S.; Hodes, G.; Calzaferri, G. The Silver Chloride Photoanode in Photoelectrochemical Water Splitting. *J. Phys. Chem. B* **2002**, *106* (49), 12764−12775.
(30) Sambhy, V.; MacBride, M. M.; Peterson, B. R.; Sen, A. Silver Bromide Nanoparticle/Polymer Composites: Dual Action Tunable Antimicrobial Materials. *J. Am. Chem. Soc.* **2006**, *128* (30), 9798−9808.
(31) Li, C.; Zhang, X.; Whitbourne, R. In Vitro Antimicrobial Activity of a New Antiseptic Central Venous Catheter. *Journal of Biomaterials Applications* **1999**, *13*, 206−223.
(32) Kubasheva, Z.; Sprynskyy, M.; Railean-Plugaru, V.; Pomastowski, P.; Ospanova, A.; Buszewski, B. Synthesis and Antibacterial Activity of (AgCl, Ag)NPs/Diatomite Hybrid Composite. *Materials* **2020**, *13* (15), 3409.
(33) Pourahmad, A.; Sohrabnezhad, Sh.; Kashefian, E. AgBr/NanoAlMCM-41 Visible Light Photocatalyst for Degradation of Methylene Blue Dye. *Spectrochimica Acta Part A: Molecular and Biomolecular Spectroscopy* **2010**, *77* (5), 1108−1114.
(34) Kakuta, N.; Goto, N.; Ohkita, H.; Mizushima, T. Silver Bromide as a Photocatalyst for Hydrogen Generation from CH3OH/H2O Solution. *J. Phys. Chem. B* **1999**, *103* (29), 5917−5919.
(35) Duncan, T. V. Applications of nanotechnology in food packaging and food safety: Barrier materials, antimicrobials and sensors. *J. Colloid Interface Sci.* **2011**, *363* (1), 1−24.
(36) Sim, W.; Barnard, R. T.; Blaskovich, M. A. T.; Ziora, Z. M. Antimicrobial Silver in Medicinal and Consumer Applications: A Patent Review of the Past Decade (2007−2017). *antibiotics* **2018**, *7* (4), 93.
(37) Ho, C. H.; Tobis, J.; Sprich, C.; Thoman, R.; Tiller, J. C. Nanoseparated Polymeric Networks with Multiple Antimicrobial Properties. *Advanced Materials* **2004**, *16*, 957−961.
(38) McDonnell, A. M. P.; Beving, D.; Wang, A.; Chen, W.; Yan, Y. Hydrophilic and Antimicrobial Zeolite Coatings for Gravity-Independent Water Separation. *Advanced Functional Materials* **2005**, *15*, 336−340.
(39) Anderson, K.; Butler, E.; Anderson, D.; Woolley, E. The Solubility of Silver Chloride and the Concentrations of Silver-Containing Species in Ethanol-Water Mixtures. *J. Phys. Chem.* **1967**, *71* (11), 3566−3569.
(40) Sportelli, M. C.; Clemente, M.; Izzi, M.; Volpe, A.; Ancona, A.; Picca, R. A.; Palazzo, G.; Cioffi, N. Exceptionally Stable Silver Nanoparticles Synthesized by Laser Ablation in Alcoholic Organic Solvent. *Colloids Surf., A* **2018**, *559*, 148−158.
(41) Kvítek, L.; Panáček, A.; Soukupová, J.; Kolář, M.; Večeřová, R.; Prucek, R.; Holecová, M.; Zbořil, R. Effect of Surfactants and Polymers on Stability and Antibacterial Activity of Silver Nanoparticles (NPs). *J. Phys. Chem. C* **2008**, *112* (15), 5825−5834.

https://doi.org/10.1021/acsabm.2c00207
ACS Appl. Bio Mater. XXXX, XXX, XXX−XXX

(42) Lee, H. J.; Lee, S. G.; Oh, E. J.; Chung, H. Y.; Han, S. I.; Kim, E. J.; Seo, S. Y.; Ghim, H. D.; Yeum, J. H.; Choi, J. H. Antimicrobial polyethyleneimine-silver nanoparticles in a stable colloidal dispersion. *Colloids Surf., B* **2011**, *88* (1), 505−511.
(43) Hirai, H.; Nakao, Y.; Toshima, N. Preparation of Colloidal Transition Metals in Polymers by Reduction with Alcohols or Ethers. *Journal of Macromolecular Science: Part A - Chemistry* **1979**, *13* (6), 727−750.
(44) Luo, C.; Zhang, Y.; Zeng, X.; Zeng, Y.; Wang, Y. The Role of Poly(Ethylene Glycol) in the Formation of Silver Nanoparticles. *J. Colloid Interface Sci.* **2005**, *288* (2), 444−448.
(45) Sun, X.; Dong, S.; Wang, E. One-Step Preparation of Highly Concentrated Well-Stable Gold Colloids by Direct Mix of Polyelectrolyte and HAuCl4 Aqueous Solutions at Room Temperature. *J. Colloid Interface Sci.* **2005**, *288* (1), 301−303.
(46) Sun, X.; Jiang, X.; Dong, S.; Wang, E. One-Step Synthesis and Size Control of Dendrimer-Protected Gold Nanoparticles: A Heat-Treatment-Based Strategy. *Macromol. Rapid Commun.* **2003**, *24* (17), 1024−1028.
(47) Sun, X.; Dong, S.; Wang, E. One-Step Synthesis and Characterization of Polyelectrolyte-Protected Gold Nanoparticles through a Thermal Process. *Polymer* **2004**, *45* (7), 2181−2184.
(48) Chakraborty, M.; Hsiao, F.-W.; Naskar, B.; Chang, C.-H.; Panda, A. K. Surfactant-Assisted Synthesis and Characterization of Stable Silver Bromide Nanoparticles in Aqueous Media. *Langmuir* **2012**, *28* (25), 9906.
(49) Sui, Z. M.; Chen, X.; Wang, L. Y.; Xu, L. M.; Zhuang, W. C.; Chai, Y. C.; Yang, C. J. Capping Effect of CTAB on Positively Charged Ag Nanoparticles. *Physica E: Low-dimensional Systems and Nanostructures* **2006**, *33* (2), 308−314.
(50) Majumder, S.; Naskar, B.; Ghosh, S.; Lee, C.-H.; Chang, C.-H.; Moulik, S. P.; Panda, A. K. Synthesis and characterization of surfactant stabilized nanocolloidal dispersion of silver chloride in aqueous medium. *Colloids Surf., A* **2014**, *443*, 156−163.
(51) Turetgen, I.; Vatansever, C. The Efficacy of Nano Silver Sulfadiazine and Nano Benzalkonium Chloride on Heterotrophic Biofilms. *Microbiology* **2019**, *88* (1), 94−99.
(52) Aodah, A. H.; Bakr, A. A.; Booq, R. Y.; Rahman, M. J.; Alzahrani, D. A.; Alsulami, K. A.; Alshaya, H. A.; Alsuabeyl, M. S.; Alyamani, E. J.; Tawfik, E. A. Preparation and Evaluation of Benzalkonium Chloride Hand Sanitizer as a Potential Alternative for Alcohol-Based Hand Gels. *Saudi Pharmaceutical Journal* **2021**, *29* (8), 807−814.
(53) Sarcina, L.; García-Manrique, P.; Gutiérrez, G.; Ditaranto, N.; Cioffi, N.; Matos, M.; Blanco-López, M. del C. Cu Nanoparticle-Loaded Nanovesicles with Antibiofilm Properties. Part I: Synthesis of New Hybrid Nanostructures. *Nanomaterials* **2020**, *10* (8), 1542.
(54) Lougheed, K. E. A.; Taylor, D. L.; Osborne, S. A.; Bryans, J. S.; Buxton, R. S. New Anti-Tuberculosis Agents amongst Known Drugs. *Tuberculosis* **2009**, *89* (5), 364−370.
(55) Gilbert, P.; Moore, L. E. Cationic Antiseptics: Diversity of Action under a Common Epithet. *J. Appl. Microbiol.* **2005**, *99* (4), 703−715.
(56) Delgado, A. V.; González-Caballero, F.; Hunter, R. J.; Koopal, L. K.; Lyklema, J. Measurement and Interpretation of Electrokinetic Phenomena. *J. Colloid Interface Sci.* **2007**, *309* (2), 194−224.
(57) Nocchetti, M.; Donnadio, A.; Ambrogi, V.; Andreani, P.; Bastianini, M.; Pietrella, D.; Latterini, L. Ag/AgCl Nanoparticle Decorated Layered Double Hydroxides: Synthesis, Characterization and Antimicrobial Properties. *J. Mater. Chem. B* **2013**, *1* (18), 2383−2393.
(58) Souza, T. G. F.; Ciminelli, V. S. T.; Mohallem, N. D. S. A Comparison of TEM and DLS Methods to Characterize Size Distribution of Ceramic Nanoparticles. *J. Phys.: Conf. Ser.* **2016**, *733*, 012039.
(59) Jenkins, S. I.; Pickard, M. R.; Furness, D. N.; Yiu, H. H.; Chari, D. M. Differences in Magnetic Particle Uptake by CNS Neuroglial Subclasses: Implications for Neural Tissue Engineering. *Nanomedicine* **2013**, *8* (6), 951−968.
(60) Klimonda, A.; Kowalska, I. Separation of cationic biocide by means of ultrafiltration process. *10th Conference on Interdisciplinary Problems in Environmental Protection and Engineering EKO-DOK* **2018**, *44*, 00068.
(61) Iqbal, J.; Kim, H.-J.; Yang, J.-S.; Baek, K.; Yang, J.-W. Removal of arsenic from groundwater by micellar-enhanced ultrafiltration (MEUF). *Chemosphere* **2007**, *66* (5), 970−976.
(62) Liu, H.; Zhou, X.; Zhang, X.; Shi, G.; Hu, J.; Liu, C.; Xu, B. Green Synthesis, Surface Activity, Micellar Aggregation, and Corrosion Inhibition Properties of New Gemini Quaternary Ammonium Surfactants. *Journal of Chemical & Engineering data* **2018**, *63* (5), 1304−1315.
(63) Wojciechowski, K.; Klodzinska, E. Zeta Potential Study of Biodegradable Antimicrobial Polymers. *Colloids Surf., A* **2015**, *483*, 204−208.
(64) Nguyen, T. V.; Nguyen, T. T. H.; Wang, S.-L.; Vo, T. P. K.; Nguyen, A. D. Preparation of Chitosan Nanoparticles by TPP Ionic Gelation Combined with Spray Drying, and the Antibacterial Activity of Chitosan Nanoparticles and a Chitosan Nanoparticle−Amoxicillin Complex. *Res. Chem. Intermed.* **2017**, *43* (6), 3527−3537.
(65) Zain, N. M.; Stapley, A. G. F.; Shama, G. Green Synthesis of Silver and Copper Nanoparticles Using Ascorbic Acid and Chitosan for Antimicrobial Applications. *Carbohydr. Polym.* **2014**, *112*, 195−202.
(66) Guinier, A. *Small-Angle Scattering of X-rays*; John Wiley & Sons, Inc., 1955.
(67) Gentile, L. Ferrihydrite Nanoparticles Entrapped in Shear-Induced Multilamellar Vesicles. *J. Colloid Interface Sci.* **2022**, *606*, 1890−1896.
(68) Nanda, K. K. Size-dependent density of nanoparticles and nanostructured materials. *Phys. Lett. A* **2012**, *376*, 3301−3302.
(69) Sui, Z. M.; Chen, X.; Wang, L. Y.; Xu, L. M.; Zhuang, W. C.; Chai, Y. C.; Yang, C. J. Capping effect of CTAB on positively charged Ag nanoparticles. *Physica E: Low-dimensional Systems and Nanostructures* **2006**, *33* (2), 308−314.
(70) Husein, M.; Rodil, E.; Vera, J. Formation of Silver Chloride Nanoparticles in Microemulsions by Direct Precipitation with the Surfactant Counterion. *Langmuir* **2003**, *19* (20), 8467−8474.
(71) Husein, M. M.; Rodil, E.; Vera, J. H. A Novel Method for the Preparation of Silver Chloride Nanoparticles Starting from Their Solid Powder Using Microemulsions. *J. Colloid Interface Sci.* **2005**, *288* (2), 457−467.
(72) Karimi, S.; Samimi, T. Green and simple synthesis route of Ag@ AgCl nanomaterial using green marine crude extract and its application for sensitive and selective determination of mercury. *Spectrochimica Acta Part A: Molecular and Biomolecular Spectroscopy* **2019**, *222* (5), 117216.
(73) Kou, J.; Varma, R. S. Varma, juice-induced green fabrication of Plasmonic AgCl/ag nanoparticles. *ChemSusChem* **2012**, *5*, 2435−2441.
(74) Devi, T. B.; Ahmaruzzaman, M.; Begum, S. A rapid, facile and green synthesis of ag@ AgCl nanoparticles for the effective reduction of 2, 4-dinitrophenyl hydrazine. *New J. Chem.* **2016**, *40*, 1497−1506.
(75) Zhao, X.; Zhang, J.; Wang, B.; Zada, A.; Humayun, M. Biochemical Synthesis of Ag/AgCl Nanoparticles for Visible-Light-Driven Photocatalytic Removal of Colored Dyes. *Materials* **2015**, *8* (5), 2043−2053.
(76) Adenuga, D. O.; Tichapondwa, S. M.; Chirwa, E. M. N. Facile synthesis of a Ag/AgCl/BiOCl composite photocatalyst for visible − light − driven pollutant removal. *J. Photochem. Photobiol., A* **2020**, *401* (1), 112747.
(77) Moretti, G. Auger Parameter and Wagner Plot in the Characterization of Chemical States by X-Ray Photoelectron Spectroscopy: A Review. *J. Electron Spectrosc. Relat. Phenom.* **1998**, *95* (2), 95−144.
(78) Kaushik, V. K. XPS Core Level Spectra and Auger Parameters for Some Silver Compounds. *J. Electron Spectrosc. Relat. Phenom.* **1991**, *56* (3), 273−277.
(79) Bera, S.; Gangopadhyay, P.; Nair, K. G. M.; Panigrahi, B. K.; Narasimhan, S. V. Electron Spectroscopic Analysis of Silver Nanoparticles in a Soda-Glass Matrix. *J. Electron Spectrosc. Relat. Phenom.* **2006**, *152* (1), 91−95.

https://doi.org/10.1021/acsabm.2c00207
ACS Appl. Bio Mater. XXXX, XXX, XXX−XXX

(80) Kumar, V. A.; Uchida, T.; Mizuki, T.; Nakajima, Y.; Katsube, Y.; Hanajiri, T.; Maekawa, T. Synthesis of Nanoparticles Composed of Silver and Silver Chloride for a Plasmonic Photocatalyst Using an Extract from a Weed *Solidago Altissima* (Goldenrod). *Adv. Nat. Sci: Nanosci. Nanotechnol* **2016**, *7* (1), 015002.
(81) Dong, R.; Tian, B.; Zeng, C.; Li, T.; Wang, T.; Zhang, J. Ecofriendly Synthesis and Photocatalytic Activity of Uniform Cubic Ag@AgCl Plasmonic Photocatalyst. *J. Phys. Chem. C* **2013**, *117* (1), 213−220.
(82) Bentiss, F.; Jama, C.; Mernari, B.; Attari, H. E.; Kadi, L. E.; Lebrini, M.; Traisnel, M.; Lagrenée, M. Corrosion control of mild steel using 3,5-bis(4-methoxyphenyl)-4-amino-1,2,4-triazole in normal hydrochloric acid medium. Corros. Sci. *Corrosion Science* **2009**, *51* (8), 1628−1635.
(83) Song, D.; Jin, H.; Jin, J.; Jing, D. Sedimentation of Particles and Aggregates in Colloids Considering Both Streaming and Seepage. *J. Phys. D: Appl. Phys.* **2016**, *49* (42), 425303.
(84) Midelet, J.; El-Sagheer, A. H.; Brown, T.; Kanaras, A. G.; Werts, M. H. V. The Sedimentation of Colloidal Nanoparticles in Solution and Its Study Using Quantitative Digital Photography. *Particle & Particle Systems Characterization* **2017**, *34*, 1−10.
(85) Krause, B.; Petzold, G.; Pegel, S.; Pötschke, P. Correlation of carbon nanotube dispersability in aqueous surfactant solutions and polymers. *Carbon* **2009**, *47* (3), 602−612.
(86) Khan, S. S.; Mukherjee, A.; Chandrasekaran, N. Studies on Interaction of Colloidal Silver Nanoparticles (SNPs) with Five Different Bacterial Species. *Colloids Surf., B* **2011**, *87* (1), 129−138.
(87) De Giacomo, A.; Salajkova, Z.; Dell'Aglio, M. A Quantum Chemistry Approach Based on the Analogy with π-System in Polymers for a Rapid Estimation of the Resonance Wavelength of Nanoparticle Systems. *Nanomaterials* **2019**, *9* (7), 929.

https://doi.org/10.1021/acsabm.2c00207
ACS Appl. Bio Mater. XXXX, XXX, XXX−XXX